



# Biogenic Synthesis and Characterization of Antimicrobial and Antiparasitic Zinc Oxide (ZnO) Nanoparticles Using Aqueous Extracts of the Himalayan Columbine (*Aquilegia pubiflora*)

## OPEN ACCESS

Hasnain Jan<sup>1</sup>, Muzamil Shah<sup>1</sup>, Hazrat Usman<sup>1</sup>, Muhammad Aslam Khan<sup>1,2</sup>, Muhammad Zia<sup>1</sup>, Christophe Hano<sup>3,4\*</sup> and Bilal Haider Abbasi<sup>1,3,4\*</sup>

### Edited by:

Denis Kuznetsov,  
National University of Science  
and Technology MISIS, Russia

### Reviewed by:

Michihiro Nakamura,  
Yamaguchi University, Japan  
Di Huang,  
Massachusetts Eye and Ear Infirmary  
and Harvard Medical School,  
United States

### \*Correspondence:

Christophe Hano  
christophe.hano@univ-orleans.fr  
Bilal Haider Abbasi  
bhabbasi@qau.edu.pk

### Specialty section:

This article was submitted to  
Biomaterials,  
a section of the journal  
Frontiers in Materials

Received: 02 December 2019

Accepted: 09 July 2020

Published: 12 August 2020

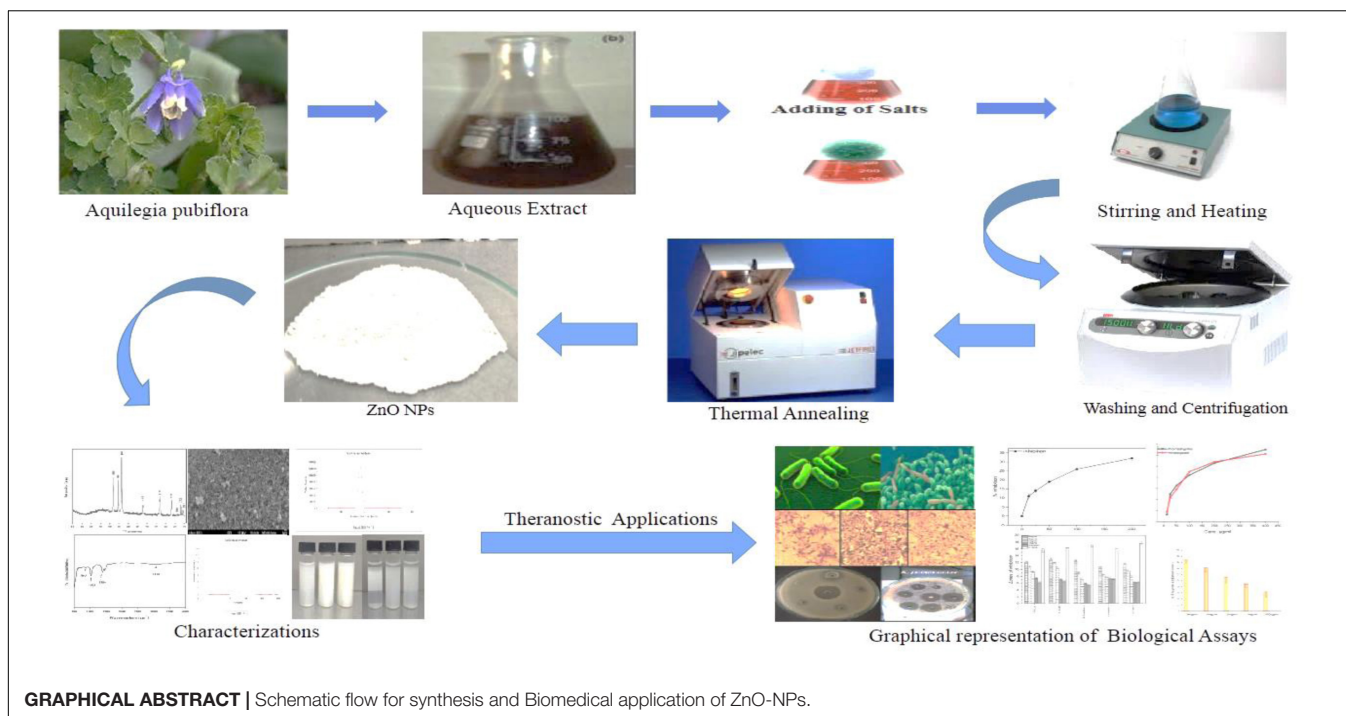
### Citation:

Jan H, Shah M, Usman H,  
Khan MA, Zia M, Hano C and  
Abbasi BH (2020) Biogenic Synthesis  
and Characterization of Antimicrobial  
and Antiparasitic Zinc Oxide (ZnO)  
Nanoparticles Using Aqueous  
Extracts of the Himalayan Columbine  
(*Aquilegia pubiflora*).  
Front. Mater. 7:249.  
doi: 10.3389/fmats.2020.00249

<sup>1</sup> Department of Biotechnology, Quaid-i-Azam University, Islamabad, Pakistan, <sup>2</sup> Department of Biotechnology, International Islamic University, Islamabad, Pakistan, <sup>3</sup> Laboratoire de Biologie des Ligneux et des Grandes Cultures, INRAE USC1328, Université d'Orléans, CEDEX2, Orléans, France, <sup>4</sup> COSMACTIFS, Bioactifs et Cosmétiques, CNRS GDR3711, Orléans, France

Herein, we report a facile, economic, one-pot green synthesis of zinc oxide nanoparticles (ZnO-NPs) for diverse biomedical applications. In the study, ZnO-NPs were synthesized using an aqueous extract of *Aquilegia pubiflora* as an effective reducing and capping agent. The biomediated nanoparticles were characterized using various techniques including high-performance liquid chromatography (HPLC), X-ray diffraction, Fourier transform infrared spectroscopy (FTIR), scanning electron microscopy, Dynamic light scattering, photoluminescence, and RAMAN. The particles were highly pure, having an average size of 34.23 nm with spherical or elliptical morphology, and displayed good aqueous dispersion capability. FTIR and HPLC confirmed the successful capping of flavonoids and hydroxycinnamic acid derivatives. The characterized NPs were then explored for their antimicrobial and anti-leishmanial potential. Among the tested bacterial and fungal strains, ZnO-NPs were more potent toward *Pseudomonas aeruginosa* and *Fusarium solani* with inhibition zone of  $10.3 \pm 0.19$  mm and  $13 \pm 1.4$  mm, respectively. A dose-dependent cytotoxic effect was observed against *Leishmania tropica* (KWH23) with significant IC<sub>50</sub> for both the promastigote (48  $\mu$ g/mL) and amastigote form (51  $\mu$ g/mL) of the parasite. In addition, bacterial kinase enzymes were inhibited by ZnO-NPs, thus allowing us to elaborate a possible action mechanism. Finally, the remarkable biocompatible nature of the particles was confirmed against freshly isolated human red blood cells (hRBCs). Altogether, these results affirmed the high antimicrobial and antiparasitic potential of ZnO-NPs obtained through a biogenic synthetic approach using aqueous extract of the Himalayan Columbine (*Aquilegia pubiflora*).

**Keywords:** zinc oxide nanoparticles, green synthesis, nanomedicine, bio-compatible, phytochemicals, antibacterial and antifungal



## INTRODUCTION

In recent years, the development of environmentally friendly techniques for the synthesis of nanoscale materials has become a major focus for material scientists (Irvani, 2011). In this regard, plant-based synthesis of NPs is a growing trend in green chemistry that is considered facile, inexpensive, and nontoxic (Bala et al., 2015; Duan et al., 2015). Over the past decade, extensive research on metal oxide NPs has been focused due to their numerous applications in various technological sectors (Altavilla and Ciliberto, 2011). Among metallic nanoparticles, zinc oxide nanoparticles (ZnO-NPs) are promising inorganic materials with multifaceted advantages. Excellent optical, semiconducting, and piezoelectric properties and chemical sensing make ZnO-NPs to be exploited across various industries such as composites, cosmetics, catalysis, energy storage, electronics, textile, and health (Hatamie et al., 2015; Kumar and Rao, 2015; Kumar et al., 2015; Al-Naamani et al., 2016; Sankapal et al., 2016). The NPs are nontoxic, biocompatible, and inexpensive and exhibit various biomedical applications including their use as antimicrobial and antiparasitic agents (Cai et al., 2016).

Currently, ZnO-NPs are commonly synthesized through physical and chemical means. The chemical approaches include sol-gel, hydrothermal, spray pyrolysis, sonochemical, solvothermal, and electrodeposition while the commonly used physical techniques include thermal evaporation, pulsed-laser deposition, molecular beam epitaxy, and chemical laser deposition (Ameen et al., 2015; Fan et al., 2015; Mani

and Rayappan, 2015; Sonker et al., 2015; Suntako, 2015; Wang et al., 2015).

Though chemical and physical methods for synthesis of ZnO-NPs offer a couple of advantages, they suffer from considerable drawbacks. The physical methods of synthesis are accompanied with high-energy requirements while chemical synthesis involves the use of noxious chemicals, making both the methods environment unfriendly, expensive, and laborious (Diallo et al., 2015).

To overcome the problems of hazardous waste and energy, green synthesis of NPs has been proposed and successfully harnessed for the synthesis of ZnO-NPs; therefore, a paradigm shift can be observed toward the bio-nano interface. Among the various biological resources (plants, bacteria, algae, and fungi), plants provide an ideal platform for the biosynthesis of NPs (Thema et al., 2015). The biogenic synthesis of ZnO-NPs has already been demonstrated; however, limited data is available on their diverse biological properties.

Here, we report a rapid, room-temperature synthesis of the ZnO-NPs via a complete environmentally friendly procedure which involves the use of aqueous extracts of *Aquilegia pubiflora* as an effective oxidizing/reducing as well as capping agent. *A. pubiflora* is an important native plant with well-documented medicinal uses. Traditionally, the plant is used for varied ailments including hepatitis, wound healing, treatment of skin burns, jaundice, and circulatory and cardiovascular diseases (Hussain et al., 2011; Adnan et al., 2012; Ahmed and Murtaza, 2015; Thatoi et al., 2016). Owing to its ease of availability and medicinal importance, the plant was employed for biosynthesis of ZnO-NPs for a broad range of therapeutic applications.

To the best of our knowledge, it is the first-ever report on *A. pubiflora*-mediated synthesis of ZnO-NPs. The NPs were well characterized by high-performance liquid chromatography (HPLC), Fourier transform infrared spectroscopy (FTIR), X-ray diffraction (XRD), scanning electron microscopy (SEM), Raman spectroscopy, and photoluminescence (PL). The well-characterized NPs were then investigated for their antimicrobial and anti-leishmanial and protein kinase (PK) inhibition potential. Moreover, to ensure the biocompatible nature hemocompatibility of the NPs against freshly isolated human red blood cells (hRBCs) was also investigated.

## MATERIALS AND METHODS

### Collection and Processing of the Plant Material

The herb reported in the current study was collected from District Swat (Main Damm), Khyber Pakhtunkhwa, Pakistan. The plant was taxonomically identified as *A. pubiflora* at the Department of botany, Bacha Khan University, Charsadda, and later on verified at the Department of Plant Sciences, Quaid-i-Azam University, Islamabad, Pakistan.

The fresh and fine leaves of the plant were excised into small pieces through a sterile surgical blade, rinsed well with distilled water to remove any dust particles and impurities, followed by shade drying. The well-dried leaves were then ground into fine powder in a Willy mill and stored at 25°C for aqueous extraction.

Aqueous leaf extract of plant material was prepared by adding 30 g of fine powder in flasks (500 ml) containing 200 ml of distilled water, sonicated continuously for 10 min, and kept in a shaking incubator at 200 rpm for 2 days at 37°C. The prepared extract was initially filtered twice with nylon cloth to remove solid residues, and the obtained extract was further filtered using Whatman filter paper three times to remove any remaining particulates. The fresh filtrate was then processed for further use.

### HPLC Analysis

Samples were analyzed by HPLC following aqueous extraction as described above. The HPLC system was composed of a Varian HPLC system with a Varian Prostar 230 pump, a Metachem Degasit degasser, a Varian Prostar 410 autosampler, and a Varian Prostar 335 Photodiode Array Detector (PAD). The HPLC system was driven by Galaxie version 1.9.3.2 software (Varian, Le Plessis-Robinson, France). HPLC-grade standards were obtained from Sigma-Aldrich. The technique used for separation is adapted from Bourgeois et al. (2016). Here, Hypersil PEP 300 C18, 250 × 4.6 mm, 5 μm particle size equipped with a guard column Alltech, 10 × 4.1 mm, was used at 35°C. Compound detection was achieved at 280 nm. The mobile phase was composed of a mixture of solvent A = HCOOH/H<sub>2</sub>O, pH = 2.1, and solvent B = CH<sub>3</sub>OH (HPLC-grade solvents). The mobile-phase composition varied during a 1-h run, with a nonlinear gradient as follows: 8% B (0 min), 12% B (11 min), 30% B (17 min), 33% B (28 min), 100% B (30–35 min), and 8% B (36 min) at a flow rate of 1 mL/min. A 10-min re-equilibration was applied between each run. Quantification was based on

external 5-point calibration curves with  $R^2$  of at least 0.999 using commercial reference standards (Sigma-Aldrich; **Table 1**). All the samples were analyzed thrice, and the results expressed in μg/mg DW of the sample.

### Biosynthesis of ZnO Nanoparticles

Zinc oxide nanoparticles were synthesized according to a previously described protocol with slight modifications (Thema et al., 2015). Briefly, 6.0 grams of zinc acetate dihydrate (Zn (CH<sub>3</sub>COO)<sub>2</sub>·2H<sub>2</sub>O (Sigma-Aldrich) was added to 100 ml extract and kept on a magnetic stirrer at 60°C for 2 h. Once the reaction was completed, the mixture was allowed to cool down at 25°C, centrifuged (HERMLE Z326K) at 10,000 rpm for 10 min. The supernatant was discarded and the remaining pellet was washed thrice with distilled water, poured into a clean Petri plate, and oven-dried at 90°C. The dried material was then grounded into fine powder in pestle and mortar and calcinated for 2 h at 500°C to remove any impurities. The annealed powder was stored in an airtight glass vial, labeled as ZnO-NPs, and was further used for physical characterization and biological applications.

### Physicochemical and Morphological Characterization

Several characterization techniques including XRD, FTIR, PL, SEM, RAMAN spectroscopy, dynamic light scattering (DLS), and dispersion studies were carried out to evaluate the structural, chemical, vibrational, and morphological properties of biosynthesized ZnO-NPs. To determine the crystalline nature, XRD (Model-D8 Advance, Germany) was carried out in the range of 2 θ (10°–80°) with a step time of 0.55 s and scanning step size of 0.03 °/s. Diffraction data were obtained through Cu Kα radiation (wavelength, 1.5406 Å; generator voltage, 40 kV; and tube current, 30 mA). About 1 mg of powdered ZnO-NPs was used for analysis. To calculate the crystallite size, Scherer's equation was used as follows:

$$D = K\lambda/\beta\cos\theta$$

where D denotes crystallite size,  $k$  represents the shape factor (0.94),  $\lambda$  depicts the X-ray wavelength which was 1.5421 Å, and  $\beta$  and  $\theta$  refer to the full width at half maximum in radians and Bragg's angle, respectively. To determine the associated functional groups on NPs, with capping and reducing agents within the extract as a result, FTIR and HPLC were carried out. The dispersion stability of the particles was investigated visually in distilled water with varied pH as a function of storage time. Morphological attributes were examined through SEM. DLS of biogenic ZnO-NPs was performed to determine the zeta potential and size distribution. RAMAN spectroscopy of biogenic ZnO-NPs was performed in the spectral range of 200 to 700 cm<sup>-1</sup> to find the vibrational modes of NPs while room temperature PL spectra were determined in the spectral range of 500 to 900 nm.

### Antibacterial Assay

The agar well diffusion method, as documented, previously was used with some modifications for the assessment of *in vitro* bactericidal potential of ZnO-NPs against different

bacterial strains (Thatoi et al., 2016). The seeding density ( $1 \times 10^6$  CFU/mL) of the bacterial culture was optimized. 50  $\mu$ L of refreshed cultures in nutrient broth was used to prepare lawn on the nutrient agar plates. Each well was carefully filled with 10  $\mu$ L of the test sample. Accordingly, the seeded plates were labeled. Cefixime and roxithromycin (standard antibiotics), and DMSO acted as positive and negative controls, respectively. After incubation for 24 h at 37°C, each well loaded with tested samples and positive–negative controls were checked for the appearance of a zone of inhibition (ZOI). The diameter of zones was measured in mm with a Vernier caliper.

### Antifungal Assay

The agar well diffusion method (Ahmad et al., 2016) with slight modifications, was used to evaluate the antifungal potency of ZnO-NPs. In brief, a sterile SDA medium was poured in autoclaved plates and a 100- $\mu$ L spore suspension of every fungal strain was taken and swabbed on solidified media in Petri plates. Each tested sample (10  $\mu$ L) was applied into sterilized wells in the agar plates. The seeded plates were labeled accordingly. DMSO and clotrimazole were carried as negative and positive control, respectively. Plates were incubated at 28°C for 24–48 h to visualize the fungal growth. After incubation, each loaded disk with tested samples, and controls was checked for the appearance of ZOI (zone of inhibition). The diameter of ZOI was measured using a Vernier caliper to the nearest mm.

### Protein Kinase Assay

Protein kinase enzyme inhibition assay was performed to verify the PK inhibition ability of anti-cancerous potentials of biogenic ZnO-NPs with slight modifications in protocol elucidated by Fatima et al. (2015). A medium (TSB broth) was made ready, autoclaved at 121°C for 20 min, and incubated for 24 h to confirm any impurity. Both *Streptomyces* strains and autoclaved TSB broth were kept in a shaking incubator at 30°C for 24 h. Except for agar, starch, and calcium carbonate, all the remaining ingredients were added with 300 mL of distilled water and mixed constantly with a stirrer. Starch, calcium carbonate, and agar were dissolved in 200 mL of distilled water in a separate flask. Both the solutions were finally mixed to make the final concentration of 500 mL. The medium was autoclaved and emptied to autoclaved Petri plates under antiseptic conditions to avoid contamination. The medium was kept solidified, and *Streptomyces* strain in the culture broth was uniformly spread on the surface of the media with autoclaved cotton buds. A sterile borer was used for making wells, and molten agarose was added to the bottom of the wells to avoid diffusion of the test samples. Afterward, 20  $\mu$ L of the serially diluted sample was added to each well and kept intact for a few minutes to avoid aggregation of the poured sample in wells. Surfactin was assessed as positive control. Petri plates were properly labeled and kept for incubation at 37°C for 24–48 h. Using a Vernier caliper, zones of inhibition were measured in mm after 48 h, respectively.

### Anti-leishmanial Assay

The anti-leishmanial potential of the biogenic ZnO-NPs was assessed against the amastigote and promastigote cultures of

*L. tropica* KWH23 (Department of Biotechnology, BKUC, Pakistan; Ahmad et al., 2015). M199 media having 10% fetal bovine serum helped in the culture of leishmanial parasites. *Leishmania* culture at a density of  $1 \times 10^6$  cells/mL was used for the analysis. The activity was executed in a 96-well plate with concentrations ranging from 400 to 25  $\mu$ g/mL. DMSO was used as blank, and amphotericin was used as a positive control. The seeded 96-well plate with test dilutions was incubated at room temperature for 72 h. OD was noted at 540 nm, while all the lived cultures were counted using an inverted microscope, and their LC<sub>50</sub> values were calculated by applying TableCurve software. Percent inhibition was measured as

$$\% \text{ Inhibition} = \left[ 1 - \left\{ \frac{\text{Absorbance of sample}}{\text{Absorbance of control}} \right\} \right] \times 100$$

### Biocompatibility of ZnO Nanoparticles With RBCs

The biocompatibility of ZnO-NPs was probed against freshly isolated hRBCs to assess the bio-safe nature (Matinise et al., 2017). About 1 mL of blood was collected from healthy individuals with informed consent. The isolated blood was poured in the EDTA tube to prevent blood clotting. For isolation of erythrocytes, blood was centrifuged at 12,000 rpm for 7 min. Once centrifugation was completed, the supernatant was discarded, and the remaining pellet was washed three times with phosphate-buffered saline (PBS). 200  $\mu$ L of erythrocyte suspension was mixed with 9.8 mL of PBS (pH: 7.2) and gently shook for preparing PBS–erythrocyte suspension. Different concentrations of NPs along with prepared erythrocyte suspension were taken in eppendorf tubes and incubated for 1 h at 35°C. All the reaction mixtures were centrifuged at 10,000 rpm for 10 min after incubation. 200  $\mu$ L of the supernatant was transferred from each tested sample in a 96-well plate, and absorption was recorded for hemoglobin release at 540 nm (0.5%). Triton X-100 was used as a positive control while DMSO was employed as a negative control. Percentage hemolysis was calculated as

$$(\%) \text{ Haemolysis} = \left( \frac{\text{sample} - \text{negative control}}{\text{Positive control} - \text{Negative control}} \right) \times 100$$

## RESULTS AND DISCUSSION

### Synthesis and HPLC Analysis of Green ZnO-NPs

In the current study, an aqueous leaf extract of *A. pubiflora* was utilized as a reducing and stabilizing agent for the synthesis of multifunctional ZnO-NPs. To the best of our knowledge, it is the first-ever study on *A. pubiflora*-mediated synthesis of metallic nanoparticles. Genus *Aquilegia* belongs to the family Ranunculaceae that has more than 60 plant species, which are used for several medicinal purposes around the world, mainly in South Asia. The species are rich in medicinally important phytochemicals including aquilegionolide, apigenin,  $\beta$ -sitosterol, berberine, caffeic acid, genkwanin, glochidionolactone A, ferulic

**TABLE 1** | Quantification parameters of the HPLC method used.

Compound	RT (min)	$\lambda_{\text{max}}$ (nm)	Linear range (mg/L)	Equation	$R^2$	LOD (mg/L)	LOQ (mg/L)
Sinapic acid	18.75	295	0.5–200	$y = 8.1529x + 0.962$	0.9996	0.18	0.60
Ferulic acid	21.34	295	0.5–200	$y = 13.123x + 1.376$	0.9994	0.17	0.57
Chlorogenic acid	25.67	325	0.5–200	$y = 5.041x + 0.324$	0.9997	0.22	0.73
<i>p</i> -Coumaric acid	27.31	325	0.5–200	$y = 7.561x + 0.623$	0.9992	0.14	0.47
Orientin	36.45	350	0.5–200	$y = 22.456x + 0.456$	0.9998	0.24	0.79
Isoorientin	37.87	350	0.5–200	$y = 25.872x + 0.634$	0.9998	0.11	0.37
Vexitin	43.23	335	0.5–200	$y = 26.327x + 1.878$	0.9998	0.18	0.59
Isovitexin	48.12	335	0.5–200	$y = 28.348x + 1.437$	0.9999	0.21	0.71

acid, magnoflorine, *p*-coumaric acid, and resorcylic acid (Bylka et al., 2002; Yu et al., 2007; Mushtaq et al., 2016). These phytochemicals including phenolics and flavonoids could have played an essential role in the synthesis of stable nanoparticles. To determine and quantify the specific phytochemicals responsible for reducing and successful capping, HPLC was performed. A total of eight compounds including four flavonoids (vitexin, isovitexin, orientin, and isoorientin) and four hydroxycinnamic acid derivatives (sinapic acid, chlorogenic acid, ferulic acid, and *p*-coumaric acid) were detected and quantified for both aqueous leaf extract and synthesized ZnO-NPs, as shown in **Figure 1**. Flavonoids and hydroxycinnamic acids are phenolics, produced through the shikimic acid pathway and are responsible for performing various biological activities of plants (Nazir et al., 2019; Santos-Sánchez et al., 2019; Usman et al., 2020). HPLC results (**Table 1**) indicate the presence of higher

concentrations of both flavonoids and hydroxycinnamic acid derivatives for leaf extract as compared to ZnO-NPs (**Table 2**). Among the detected flavonoids, orientin was observed to be present in higher concentrations for both leaf extract and ZnO-NPs (707.56  $\mu\text{g/g}$  DW and 45.59  $\mu\text{g/g}$  DW, respectively) while chlorogenic acid was found to be abundant hydroxycinnamic acid for both leaf extract (1.70  $\mu\text{g/g}$  DW) and ZnO-NPs (0.129  $\mu\text{g/g}$  DW) as compared to other hydroxycinnamic acid derivatives. Orientin and chlorogenic acid protect the plant from stress conditions and perform various biological activities such as antioxidant, antiaging, anti-inflammatory, antidiabetic, antifungal, antibacterial, hepatoprotective, and anticancer (Lam et al., 2016; Naveed et al., 2018). The presence of flavonoids and hydroxycinnamic acid derivatives on the surface of nanoparticles is according to the results of our previous reports (Jan et al., 2020; Shah et al., 2020). These

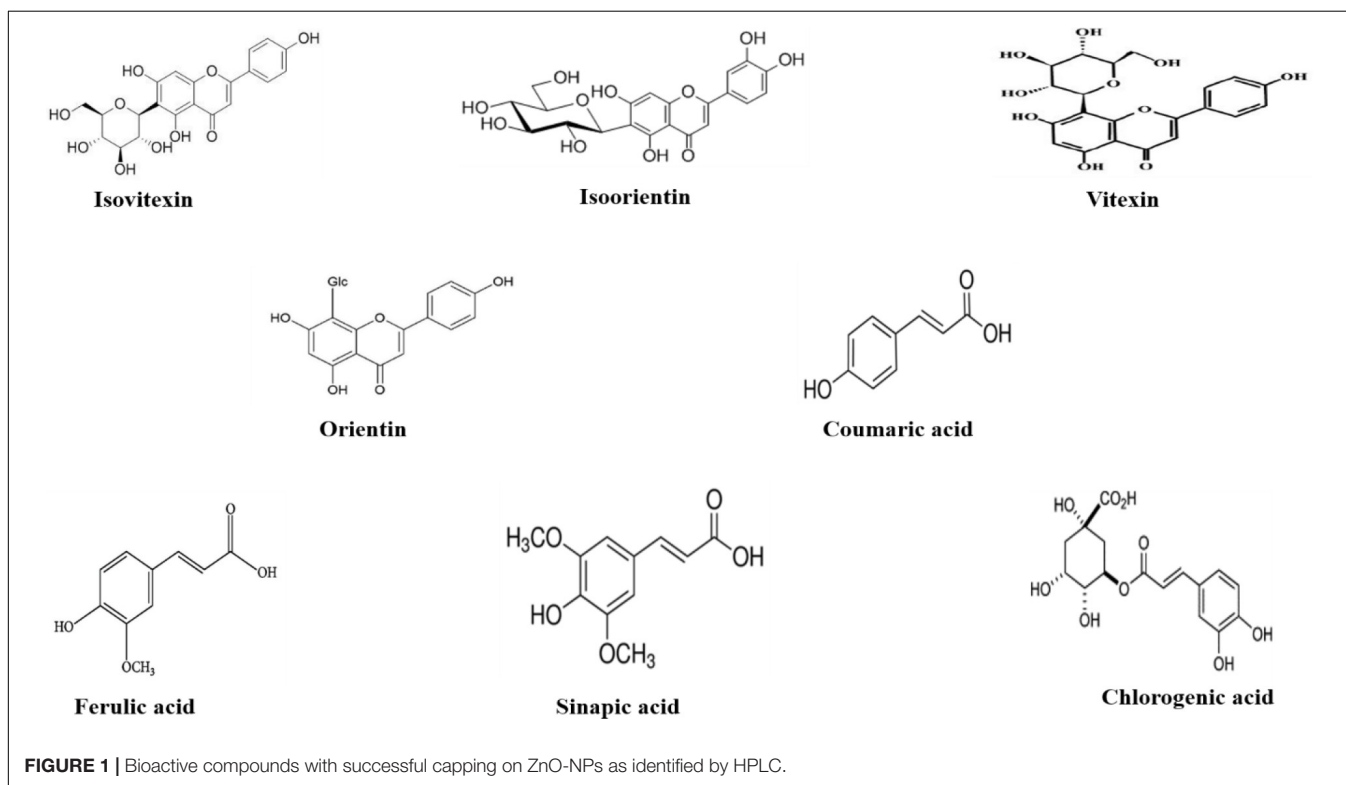


**TABLE 2** | HPLC analysis of the *A. publiffora* leaf extract and biosynthesized ZnO-NPs.

Phytochemicals	Leaf extract ( $\mu\text{g/g DW}$ )	ZnO-NPs ( $\mu\text{g/g DW}$ )
<b>Flavonoids</b>		
Orientin	707.56 $\pm$ 5.09	45.59 $\pm$ 2.10
Isoorientin	351.43 $\pm$ 3.02	13.03 $\pm$ 1.09
Isovitexin	390.65 $\pm$ 3.65	8.14 $\pm$ 0.98
Vitexin	111.39 $\pm$ 2.71	nd
<b>Hydroxycinnamic acids</b>		
<i>p</i> -Coumaric acid	0.22 $\pm$ 0.034	0.038 $\pm$ 0.006
Ferulic acid	0.43 $\pm$ 0.065	0.043 $\pm$ 0.009
Sinapic acid	0.16 $\pm$ 0.014	0.038 $\pm$ 0.004
Chlorogenic acid	1.70 $\pm$ 0.13	0.129 $\pm$ 0.008

Values are means  $\pm$  standard deviations (SD) of 3 independent experiments. nd: not detected (below the LOD).

plant active compounds are considered to be involved in the capping of ZnO-NPs, as shown in **Figure 2**. After subsequent steps of washing, drying, grinding, and calcination, white powder of ZnO-NPs was obtained. The fine powder collected was stored in an airtight glass vial, labeled as ZnO-NPs, and was stored at room temperature for physicochemical, morphological characterization, and biological applications.

## Physicochemical and Morphological Characterization

### XRD (X-Ray Diffraction) Analysis

The phase identification, structure, and purity of the biosynthesized ZnO-NPs were investigated through XRD. The XRD pattern (**Figure 3A**) confirmed the pure and crystalline nature of nanoparticles with strong diffraction peaks observed at different  $2\theta$ , i.e., 31.74, 34.34, 36.36, 47.39, 56.31, 62.68, 66.83, 68.23, and 69.47°, corresponding to different miller indices

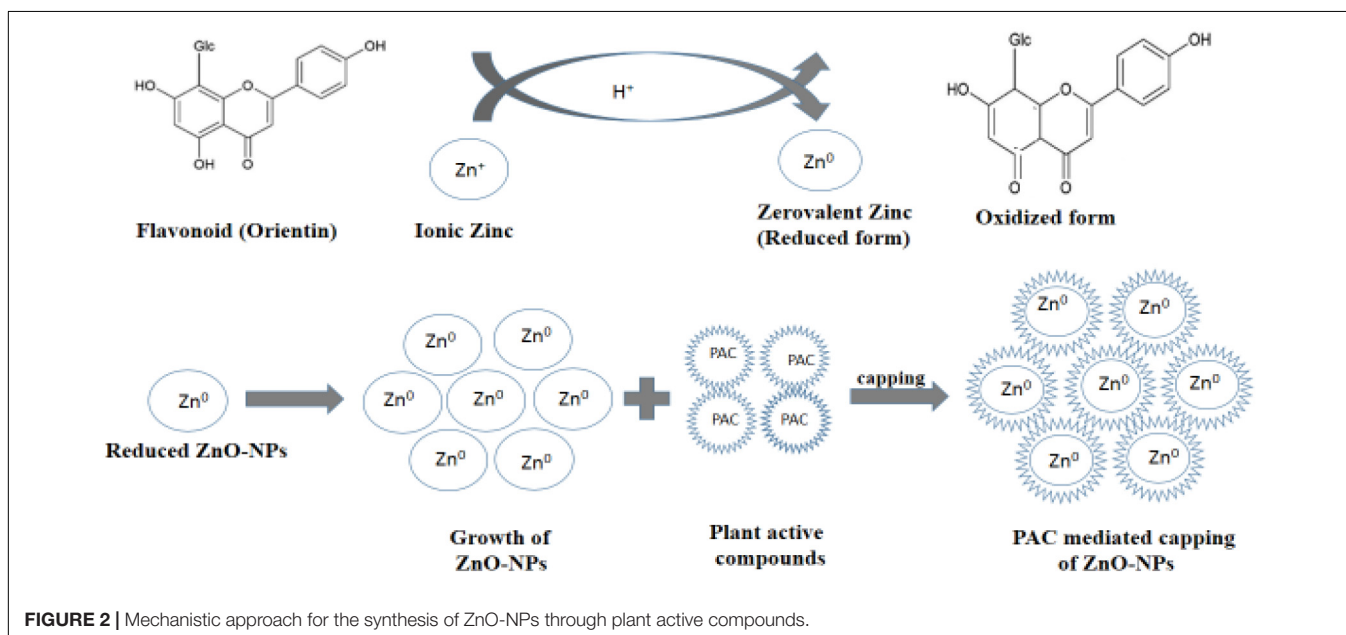
(100), (002), (101), (102), (110), (103), (200), (212), and (201), respectively. The indexation confirms the standard hexagonal wurtzite structure (JCPDF file no. 00-036-1451) of ZnO-NPs as previously reported in other studies (Arakha et al., 2015; Janaki et al., 2015; Vijayakumar et al., 2016; Matinise et al., 2017). Moreover, the average crystallite size as calculated by Scherer's equation was found to be 19.58 nm.

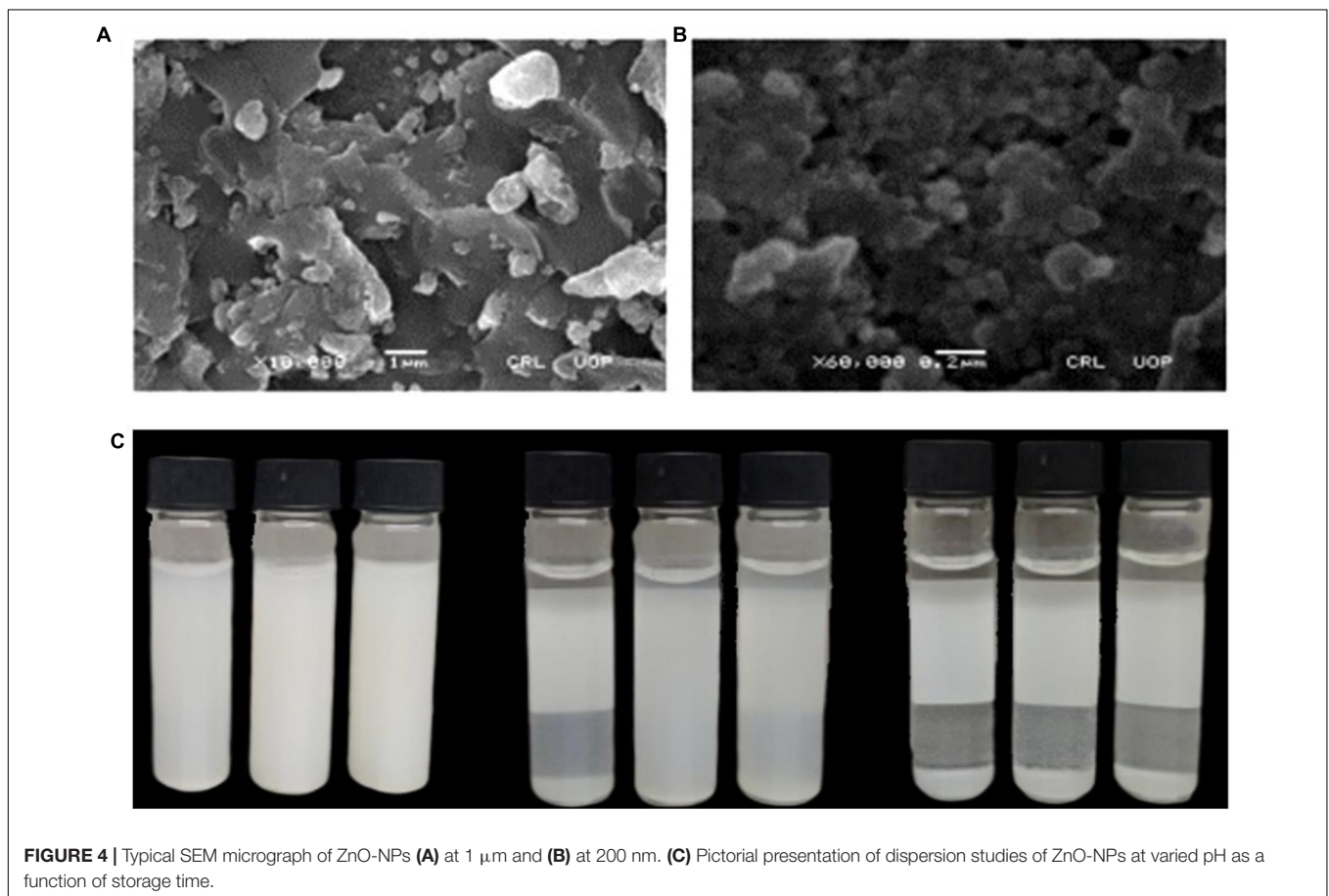
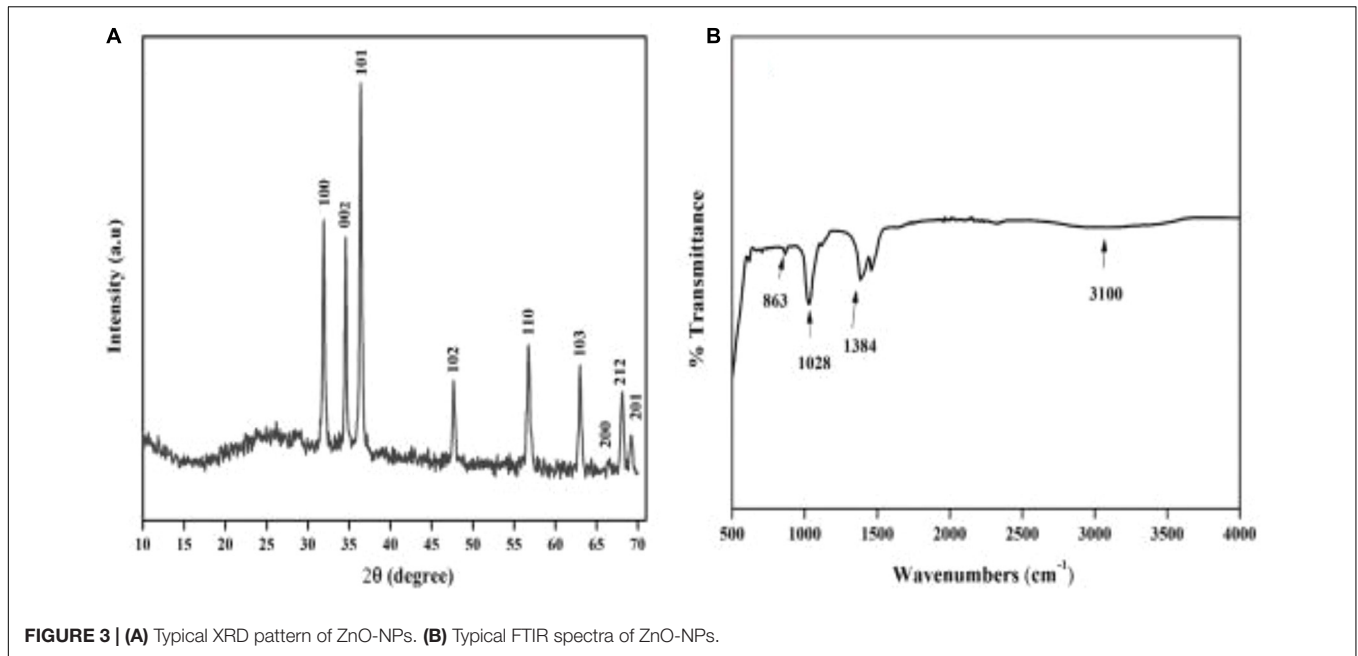
### Fourier Transform Infrared Spectroscopy

Fourier transform infrared spectroscopy was used to examine the surface adsorption of functional groups on biosynthesized nanoparticles. **Figure 3B** depicts typical FTIR spectra in the spectral range of 400–4000  $\text{cm}^{-1}$ . The major absorption peaks were observed in the region of lower wave numbers. A broad band observed at 3100  $\text{cm}^{-1}$  corresponds to the O–H stretching mode of hydroxyl groups (Vijayalakshmi et al., 2016). The peak intensity at 1459  $\text{cm}^{-1}$  showed amine (–NH) vibration stretch in protein amide linkages (Jamdagni et al., 2018). The intense bands observed at 1028  $\text{cm}^{-1}$  and 1384  $\text{cm}^{-1}$  represented alcohols, phenolic groups, and C–N stretching vibrations of aromatic amines of biomolecules (Huang et al., 2007). A characteristic band observed at 863  $\text{cm}^{-1}$  corresponds to the Zn–O stretching bond (Taş et al., 2000; Sangeetha et al., 2011). FTIR spectra affirm successful capping of biomolecules on the NP surface and thus provide stability and dispersion capacity to ZnO-NPs in aqueous media.

### Scanning Electron Microscopy Analysis

The surface morphology and particle size of the green synthesized ZnO-NP were determined using SEM. **Figures 4A,B** show typical scanning electron micrograph NPs. As can be seen from the micrographs, the particles exhibit a sphere-shape morphology with extent of aggregation. Such morphologies were also reported in previous studies (Davar et al., 2015;

**FIGURE 2** | Mechanistic approach for the synthesis of ZnO-NPs through plant active compounds.



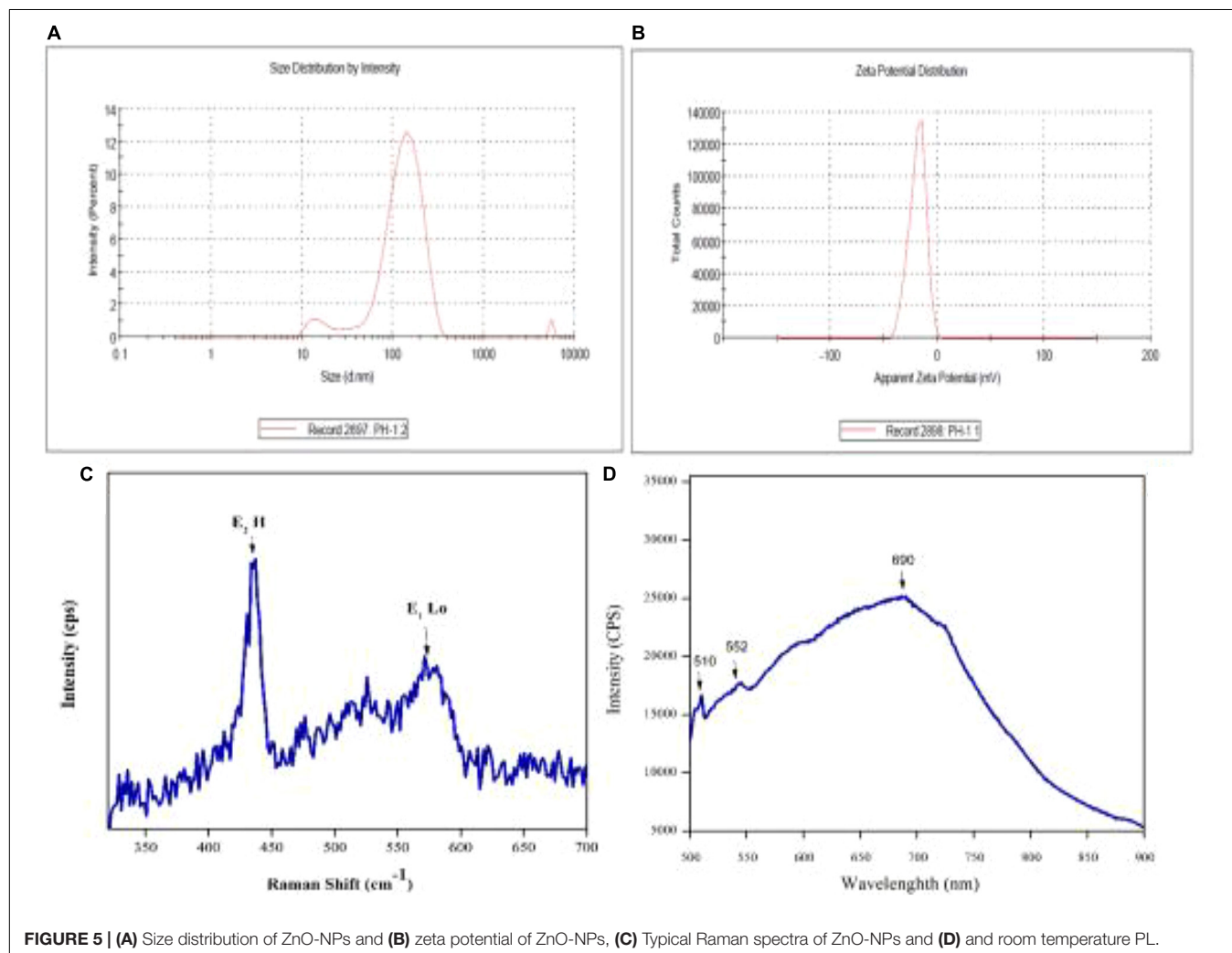
Suresh et al., 2015; Khan et al., 2018). For instance, in a study, sphere-shaped nanoparticles were reported using aqueous leaf extract of three plants, i.e., *Abutilon indicum*, *Clerodendrum infortunatum*, and *Clerodendrum inerme*. Moreover, the average particle size of the nanoparticles as calculated using ImageJ software was found to be 34.23 nm.

## Dispersion Studies

Dispersion plays a vital role in determining functional activities of the engineered nanoparticles in any biological system (Bihari et al., 2008). Several parameters affect the dispersion capacity of the nanoparticles such as presence of charged or uncharged molecules that are adsorbed on the particle surface and the ionic strength of the solvent (Modena et al., 2019). In order to investigate the dispersion capability of ZnO nanoparticles, distilled water at different pH values was used. **Figure 4C** illustrates the dispersion capacity of ZnO-NPs at pH: 2, pH: 7, and pH: 12. It was observed that ZnO exhibited excellent dispersibility at neutral pH even after 24 h of sonication. The results were later augmented by a highly negative zeta potential value at neutral pH, which quantifies the stable dispersion capability of nanoparticles.

## Dynamic Light Scattering

Zeta potential and size distribution of the particles was investigated using a Malvern zeta sizer. Zeta potential ( $\zeta$ ) is a typical measurement of the surface charge and defines colloidal stability of the particles. Suspensions that feature  $|\zeta| \geq 15$  mV are generally categorized as stable colloids (Modena et al., 2019). The zeta potential of synthesized ZnO-NPs in distilled water was recorded as  $-18.4$  mV and can thus be considered as stable colloidal solution in **Figures 5A,B**. The measurement augments and verifies the stable dispersion capability of biogenic ZnO nanoparticles in distilled water with pH 7. The negative surface charge on particles is due to the high binding affinity of the extract compounds on metallic ions conferring the particles' dispersion stability and preventing from aggregation (Vimala et al., 2014). Moreover, size distribution measurements revealed the average size of the particles to be 131 nm with a polydispersity index (PDI) of 0.340. As the graph shows, the particle size is polydispersed and is larger as compared to the SEM measurements. The larger size of the ZnO-NPs observed via DLS is due to the biasness of the technique toward measurement of larger particles (even aggregate; Modena et al., 2019).



## Photoluminescence and Raman Spectra

The photoluminescence study of engineered nanomaterials (ENMs) is important as it provides important information about the quality of the synthesized materials. **Figure 5D** illustrates room temperature PL spectra of ZnO-NPs. PL measurement was performed at excitation wavelength of 500 to 900 nm. Characteristic peaks were observed at 510, 552, and 690 nm referred to as trap-state or deep-state emission (Uthirakumar and Hong, 2009). It is proposed that the oxygen vacancies in ZnO exist in three charge states, i.e., neutral, singly ionized, and double ionized. Green emission from ZnO-NPs is due to existence of oxygen (Raoufi, 2013) related to the increase in oxygen vacancies and thus increase in PL emission. **Figure 5C** shows Raman spectra of the biosynthesized nanoparticles that displayed characteristic peaks at 435 and 572  $\text{cm}^{-1}$ . Similar Raman patterns were also reported in some previous studies (Diallo et al., 2015).

## Biological Applications

### Antibacterial Activity

Pathogenic bacteria and fungi cause a broad range of diseases in both humans and animals. Extensive research and sophisticated scientific approach have become inevitable for the establishment of new therapeutic values to overcome microbial resistance and the nonselective and unsystemic use of antibiotics. In the study, antibacterial activity of phyto-fabricated ZnO-NPs was determined against five pathogenic bacteria including two Gram-positive (*Bacillus subtilis* and *Staphylococcus epidermidis*) and three Gram-negative (*Klebsiella pneumoniae*, *Escherichia coli*, and *Pseudomonas aeruginosa*) using agar well diffusion method as shown in **Table 3**. An example of ZnO-NP activity against *S. epidermidis* is shown in **Figure 6A**. Five different concentrations (5, 4, 2, 1, and 0.5 mg/mL) were used to probe the bactericidal potential of NP formulations. In general, all the tested strains showed dose-dependent susceptibility to ZnO-NPs with *P. aeruginosa* and *B. subtilis* found to be the most susceptible. Inhibition zones measured at 5 mg/mL were  $10.3 \pm 0.19$  for *P. aeruginosa*,  $9.5 \pm 0.31$  for *Bacillus subtilis*,  $8.7 \pm 0.18$ , and  $8.7 \pm 0.23$  for both *K. pneumoniae* and *E. coli* while  $7.1 \pm 0.24$  for *S. epidermidis*. Most of the mechanistic models for antibacterial activity of ZnO-NPs are based on the surface-to-volume ratio, size, and physicochemical properties.

Though antimicrobial mechanisms of metallic nanoparticles are subject to ongoing research, few models have been demonstrated in literature that explain the inhibitory mechanism of NPs. According to the studies, the growth inhibition effect of ZnO-NPs is the result of one or a combination of the following mechanisms: (1) electrostatic interaction between microbial cell wall and ZnO-NPs leading to cell wall destruction and thus compromise of cell integrity; (ii) accumulation of ZnO-NPs and subsequent release of  $\text{Zn}^{+2}$  within the bacterial cell; and (iii) formation of reactive oxygen species (ROS; Sirelkhatim et al., 2015; Król et al., 2017). Numerous studies have suggested ROS generation as a key mechanism responsible for the antimicrobial potential of ZnO-NPs. ROS results in DNA damage, disrupting cellular membranes and proteins and ultimately leading to cell death (Raghupathi et al., 2011). Hydroxyl radical ( $\text{OH}\cdot$ ), hydrogen peroxide ( $\text{H}_2\text{O}_2$ ), and superoxide anion ( $\text{O}^{-2}$ ) are the most abundant reactive oxygen species found in aqueous suspension of ZnO-NPs. Among these,  $\text{OH}\cdot$  is the most reactive species and reacts with any type of biomolecule within the living cells. Such biochemical reactions may lead to recombination of two  $\text{OH}\cdot$  ions to form  $\text{H}_2\text{O}_2$ . Hydrogen peroxide is a relatively weak oxidizer but may also result in cell damage. Unlike  $\text{OH}\cdot$  and  $\text{H}_2\text{O}_2$ , superoxide anion radical ( $\text{O}^{-2}$ ) has weak penetration potential and is less toxic (Hameed et al., 2015). These reactive oxygen species are produced on the surface of ZnO-NPs in aqueous media. In subsequent steps, the electrons and the holes on the ZnO-NP surface interact with water ( $\text{H}_2\text{O}$ ) molecules in the surrounding medium and form  $\text{OH}\cdot$  and  $\text{H}^+$ . In separate reactions,  $\text{O}_2$  molecules yield superoxide anion ( $\text{O}^{-2}$ ), which further produces  $\text{HO}_2\cdot$  by reacting with  $\text{H}^+$ . Furthermore, the reaction between electrons generating ( $\text{HO}_2\cdot$ ) and  $\text{H}^+$  yield ( $\text{H}_2\text{O}_2$ ) molecules, which has the capacity to penetrate cellular membranes, and ultimately damage or kill the bacteria cells (Xie et al., 2011; Sirelkhatim et al., 2015).

### Antifungal Activity

The antifungal potential of *A. pubiflora*-mediated nanoparticles was measured by the agar well diffusion method. The results are summarized in **Table 4**, though biosynthesized ZnO-NPs have been extensively studied for antibacterial operations, yet limited data is available regarding its efficacy against spore forming fungi. In the current study, ZnO-NPs were evaluated against

**TABLE 3** | Antibacterial activity of ZnO-NPs against pathogenic bacterial strains.

Pathogenic bacteria	ZnO-NPs				
	5 mg/mL	4 mg/mL	2 mg/mL	1 mg/mL	500 $\mu\text{g/mL}$
<i>E. coli</i>	$8.7 \pm 0.23^{**}$	$6.6 \pm 0.24^{**}$	$6.3 \pm 0.24^*$	$4.6 \pm 0.31^{***}$	$3.7 \pm 0.21^{***}$
<i>S. epidermidis</i>	$7.1 \pm 0.24^{***}$	$6.4 \pm 0.31^{***}$	$5.5 \pm 0.32^{***}$	$4.7 \pm 0.23^*$	$3.2 \pm 0.23^{***}$
<i>K. pneumoniae</i>	$8.7 \pm 0.18^{**}$	$7.9 \pm 0.35^*$	$5.6 \pm 0.33^{**}$	$4.8 \pm 0.18^{***}$	$3.9 \pm 0.21^{***}$
<i>P. aeruginosa</i>	$10.3 \pm 0.19^*$	$7.9 \pm 0.34^*$	$5.8 \pm 0.29^*$	$5.7 \pm 0.34^*$	$5.4 \pm 0.25^*$
<i>B. subtilis</i>	$9.5 \pm 0.31^*$	$7.7 \pm 0.39^*$	$5.5 \pm 0.29^{***}$	$5.1 \pm 0.24^*$	$4.4 \pm 0.18^{**}$
Positive control (ampicillin B)	$12.8 \pm 0.43$	$11.1 \pm 0.41$	$8.9 \pm 0.34$	$8.2 \pm 0.29$	$7.3 \pm 0.31$

Star \*–\*\*\* represent; \*\*\* highly significant, \*\* slightly significant, and \* non-significant difference from control at  $P < 0.05$  by one-way ANOVA in the column. Values are mean  $\pm$  SD of triplicate.

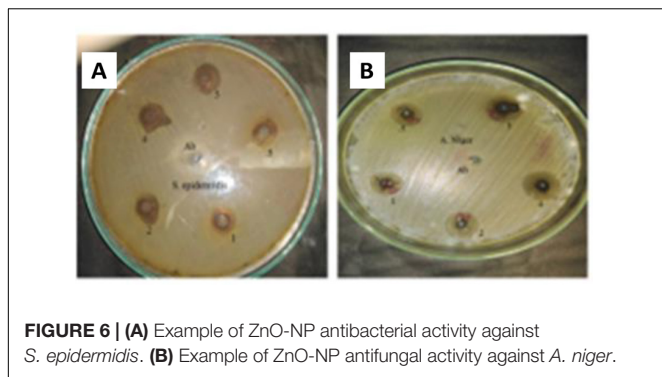


**FIGURE 6 | (A)** Example of ZnO-NP antibacterial activity against *S. epidermidis*. **(B)** Example of ZnO-NP antifungal activity against *A. niger*.

five filamentous fungal strains with stock concentrations in the range 5000–500  $\mu\text{g/ml}$ . An example of ZnO-NP activity against *A. niger* is shown in **Figure 6B**. Amphotericin B and DMSO were applied as a positive and negative control, respectively. In general, all the samples displayed dose-dependent antifungal activity. Among the tested strains, *F. solani*, *M. racemosus*, and *A. niger* showed a maximum ZOI at 5 mg/ml, which were measured as

$13 \pm 0.44$ ,  $12.7 \pm 0.39$ , and  $12.2 \pm 0.44$  mm, respectively, while the lowest ZOI was recorded  $5.4 \pm 0.24$  mm for *M. racemosus* and  $6.1 \pm 0.29$  mm for *A. niger* at 500  $\mu\text{g/ml}$ . Studies suggest that membrane disruption and free radical generation are considered as the most common methods of NP-induced cellular toxicity. ROS generation and nanoparticle interaction with fungal hyphae and spores lead to fungal growth inhibition (He et al., 2011). Significant and dose-dependent fungicidal activity has also been reported in previous studies (Sharma et al., 2010; Lipovsky et al., 2011) which is in agreement with our study. Based on the significant antibacterial and antifungal activity, ZnO-NPs can be used as an effective antimicrobial material either in pristine form or in combination or carrier for antibiotics.

### Protein Kinase Inhibition Activity

Protein kinase, a kinase enzyme, has a significant importance in anticancer therapies. The enzymes play a key role in the phosphorylation of serine–threonine and tyrosine residues; these residues are helpful in certain regulatory and controlling processes for metabolism, apoptosis of cells, and cellular proliferation/differentiation. Decontrolled phosphorylation can

**TABLE 4 |** Antifungal activity of CeO<sub>2</sub>-NPs against pathogenic fungi.

Pathogenic fungi	ZnO-NPs				
	5 mg/mL	4 mg/mL	2 mg/mL	1 mg/mL	500 $\mu\text{g/mL}$
<i>A. niger</i>	$12.2 \pm 0.44^*$	$10.1 \pm 0.43^*$	$7.5 \pm 0.26^*$	$6.4 \pm 0.21^*$	$6.1 \pm 0.29^*$
<i>M. racemosus</i>	$12.7 \pm 0.39^*$	$9.1 \pm 0.37^{**}$	$7.3 \pm 0.33^*$	$5.7 \pm 0.27^{**}$	$5.4 \pm 0.24^{**}$
<i>F. solani</i>	$13.0 \pm 0.44^*$	$10.3 \pm 0.42^*$	$7.7 \pm 0.39^*$	$6.3 \pm 0.23^*$	$5.1 \pm 0.21^{**}$
<i>A. flavus</i>	$11.1 \pm 0.41^{**}$	$9.4 \pm 0.49^{**}$	$7.1 \pm 0.31^{**}$	$5.7 \pm 0.36^{**}$	$4.8 \pm 0.25^{***}$
<i>A. fumigatus</i>	$10.7 \pm 0.34^{***}$	$8.1 \pm 0.24^{***}$	$6.2 \pm 0.34^{***}$	$5.5 \pm 0.29^{***}$	$3.7 \pm 0.28^{***}$
Positive control (Amphotericin B)	$16.6 \pm 0.54$	$12.9 \pm 0.42$	$10.4 \pm 0.38$	$10.1 \pm 0.46$	$8.8 \pm 0.31$

Star \*–\*\*\* represent; \*\*\* highly significant, \*\* slightly significant, and \* non-significant difference from control at  $P < 0.05$  by one-way ANOVA in the column. Values are mean  $\pm$  SD of triplicate.

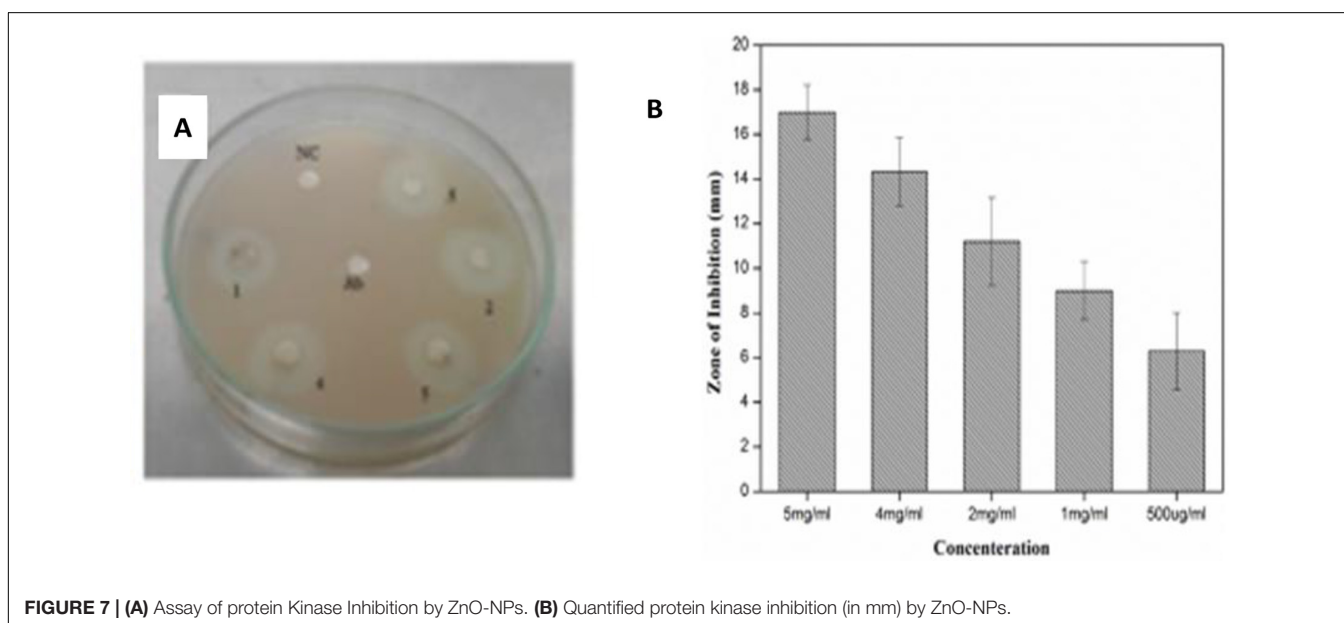
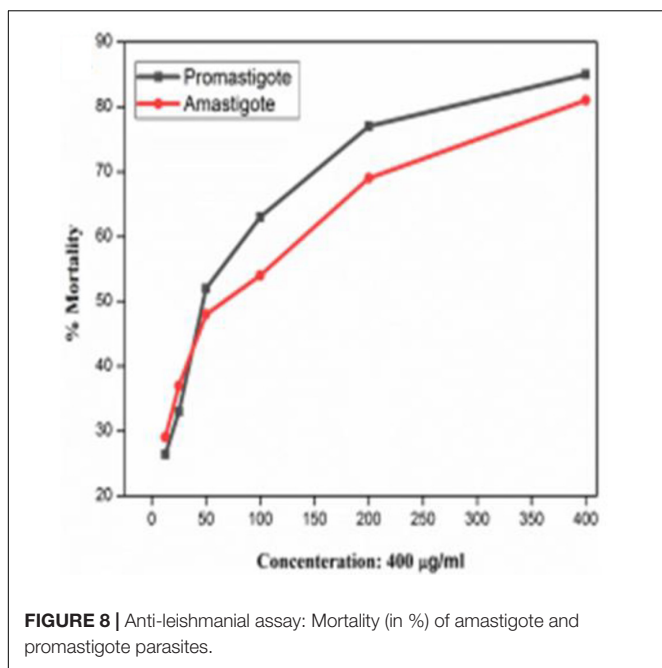


**FIGURE 7 | (A)** Assay of protein Kinase Inhibition by ZnO-NPs. **(B)** Quantified protein kinase inhibition (in mm) by ZnO-NPs.



cause and induce genetic abnormalities, leading to tumorigenesis. Therefore, all those products which have the ability to deter PK enzymes can be of significant importance in cancer research (Yao et al., 2011). PK phosphorylation also plays a vital role in the formation of hyphae in *Streptomyces* fungal strains, and the same principal is applied to determine the PK inhibition activity. The *Streptomyces* 85E strain was used to investigate medicinal compounds for investigation of the PK inhibition (Waters et al., 2002). For the preliminary anticancer screening, ZnO-NPs in different concentration were evaluated for PK inhibition. DMSO and surfactin were used as negative and positive controls, respectively. Like antimicrobial activity, ZnO-NPs also displayed dose-dependent potential against PK and the highest ZOI was observed on 5 mg/mL as  $17 \pm 1.22$  mm while the lowest ZOI was recorded as  $6.3 \pm 1.72$  mm at 500-µg/ml concentrations, respectively, as shown in **Figure 7**. Such an excellent activity of ZnO-NPs is a preliminary indication of its anticancer potential and can be considered for detailed *in vitro* and *in vivo* anticancer studies.

### Anti-leishmanial Assay

Leishmaniasis is a tropical and subtropical disease with annual incidence of 1.5 to 2 million cases worldwide. According to the World Health Organization (WHO), the disease is endemic in 89 countries and results in 70,000 deaths each year. The disease is caused by an intracellular parasite and is transmitted to humans by sand fly (phlebotomies and *Lutzomyia*) bite. Due to the inappropriate vector and inefficient and affordable drugs, the disease is at high risk of uncontrolled spreading. Recently, metal-oxide nanoparticle (oxides of zinc, silver, titanium, and magnesium)-based treatments have gained popularity because of their significant cytotoxic potential against *Leishmania* (Jebali and Kazemi, 2013). However, biosynthesized ZnO-NPs have

**TABLE 5 |** % Hemolytic analysis of *A. pubiflora* synthesized ZnO-NPs.

S.NO	Concentration (µg/mL)	% Hemolysis
1	400	$1.24 \pm 0.14^a$
2	200	$1.05 \pm 0.12^{a,b}$
3	100	$0.73 \pm 0.1^{b,c}$
4	50	$0.48 \pm 0.23^c$

Values are means  $\pm$  standard deviations (SD) of 3 independent experiments. Different letters represent significant differences between the various extraction conditions ( $p < 0.05$ ).

been rarely explored for their cytotoxicity against the parasite *Leishmania tropica* (KWH23). In the current study, ZnO-NPs in the range of 12.5–400 µg/mL were investigated via MTT cytotoxic assay against the promastigote and amastigote axenic cultures of *L. tropica* (**Figure 8**). ZnO-NP formulations were found to have dose-dependent lethality with significant mortality of  $85\% \pm 2.7$  and  $81\% \pm 3.1$  at 400 µg/mL against the parasite in promastigote and amastigote form, its morphological form being round-shaped in human host. Least mortality observed was  $26.43\% \pm 2.4$  and  $29.07\% \pm 2.9$  at the tested concentration of 12.5 µg/mL. The  $IC_{50}$  values were calculated as 48 µg/mL for promastigote and 51 µg/mL for amastigote. Our findings are in agreement with previous studies and thus emphasize on the futuristic possibilities for ZnO-NPs in anti-leishmanial therapies.

### Biocompatibility Studies of ZnO-NPs

Biocompatibility of ENMs is a key requirement for their multifaceted biomedical applications. To evaluate the bio-safe nature, ZnO-NPs were investigated for their compatibility against hRBCs. In the experiment, freshly isolated hRBCs and NP formulations were co-incubated in PBS that mimic the extracellular environment (Evans et al., 2013). The assay is based on the release of hemoglobin from red blood cells (RBCs), which can be induced by the test sample if it has the capability to rupture RBCs. The RBCs lysis is then quantified by measuring the hemoglobin release in the medium spectrophotometrically (405 nm; Amin and Dannenfeler, 2006). The NPs were screened at 400 µg/mL for hemolytic activity, shown in **Table 5**. Generally, any hemolysis  $\geq 25\%$  is considered hemolytic while hemolysis  $\leq 10\%$  is considered nonhemolytic. In the current study, ZnO-NPs exhibited remarkable hemocompatibility even at the highest tested concentration. The study thus concludes that *A. pubiflora* ZnO-NPs are highly biocompatible and can be used for diverse biomedical applications.

### CONCLUSION

The recent research work is focused on the bioaugmented synthesis of ZnO-NPs using aqueous extract of medicinally important *A. pubiflora*. The crystalline nature of the synthesized NPs was confirmed by XRD analysis. HPLC and FTIR analysis confirmed the presence of phytochemicals involved during the conversion of metallic ions into nanoparticles. Morphology and vibrational modes were determined through SEM and RAMAN spectra, while surface charge and stability were

determined through DLS. Synthesized ZnO-NPs showed effective antimicrobial (antibacterial and antifungal) and antiparasitic (anti-leishmanial) activities. The bioengineered ZnO-NPs have also exhibited an effective inhibitory potential against microbial PKs. It was also found that synthesized ZnO-NPs are biocompatible with hRBCs. Our experimental work concluded that the abovementioned ZnO-NPs have a great potential for various cosmetic or medicinal applications as biocompatible antimicrobial and antiparasitic agents. However, further research on ZnO-NPs to exploit its biomedical potential on both *in vitro* and *in vivo* levels has to be conducted.

## DATA AVAILABILITY STATEMENT

The raw data supporting the conclusions of this article will be made available by the authors, without undue reservation, to any qualified researcher.

## REFERENCES

- Adnan, M., Begum, S., Khan, A. L., Tareen, A. M., and Lee, I.-J. (2012). Medicinal plants and their uses in selected temperate zones of Pakistani Hindukush-Himalaya. *J. Med. Plants Res.* 6, 4113–4127.
- Ahmad, A., Syed, F., Shah, A., Khan, Z., Tahir, K., Khan, A. U., et al. (2015). Silver and gold nanoparticles from *Sargentodoxa cuneata*: synthesis, characterization and antileishmanial activity. *RSC Adv.* 5, 73793–73806. doi: 10.1039/c5ra13206a
- Ahmad, K., Talha Khalil, A., and Somayya, R. (2016). Antifungal, phytotoxic and hemagglutination activity of methanolic extracts of *Ocimum basilicum*. *J. Tradit. Chin. Med.* 36, 794–798. doi: 10.1016/s0254-6272(17)30017-1
- Ahmed, M. J., and Murtaza, G. (2015). A study of medicinal plants used as ethnoveterinary: harnessing potential phytotherapy in Bheri, District Muzaffarabad (Pakistan). *J. Ethnopharmacol.* 159, 209–214. doi: 10.1016/j.jep.2014.11.016
- Al-Naamani, L., Dobretsov, S., and Dutta, J. (2016). Chitosan-zinc oxide nanoparticle composite coating for active food packaging applications. *Innovat. Food Sci. Emerg. Technol.* 38, 231–237. doi: 10.1016/j.ifset.2016.10.010
- Altavilla, C., and Ciliberto, E. (2011). “Inorganic nanoparticles: synthesis, applications, and perspectives,” in *An Overview. Inorganic Nanoparticles: Synthesis, Applications, and Perspectives*, eds C. Altavilla and E. Ciliberto (New York, NY: CRC Press), 1–17.
- Ameen, S., Akhtar, M. S., and Shin, H. S. (2015). Highly dense ZnO nanowhiskers for the low level detection of p-hydroquinone. *Mater. Lett.* 155, 82–86. doi: 10.1016/j.matlet.2015.04.111
- Amin, K., and Dannenfelser, R. M. (2006). In vitro hemolysis: guidance for the pharmaceutical scientist. *J. Pharm. Sci.* 95, 1173–1176. doi: 10.1002/jps.20627
- Arakha, M., Saleem, M., Mallick, B. C., and Jha, S. (2015). The effects of interfacial potential on antimicrobial propensity of ZnO nanoparticle. *Sci. Rep.* 5:9578.
- Bala, N., Saha, S., Chakraborty, M., Maiti, M., Das, S., Basu, R., et al. (2015). Green synthesis of zinc oxide nanoparticles using Hibiscus subdariffa leaf extract: effect of temperature on synthesis, anti-bacterial activity and anti-diabetic activity. *RSC Adv.* 5, 4993–5003. doi: 10.1039/c4ra12784f
- Bihari, P., Vippola, M., Schultes, S., Praetner, M., Khandoga, A. G., Reichel, C. A., et al. (2008). Optimized dispersion of nanoparticles for biological in vitro and in vivo studies. *Part. Fibre Toxicol.* 5:14. doi: 10.1186/1743-8977-5-14
- Bourgeois, C., Leclerc, É. A., Corbin, C., Doussot, J., Serrano, V., Vanier, J.-R., et al. (2016). Nettle (*Urtica dioica* L.) as a source of antioxidant and anti-aging phytochemicals for cosmetic applications. *Compt. Rend. Chimie* 19, 1090–1100. doi: 10.1016/j.crci.2016.03.019

## ETHICS STATEMENT

Ethical review and approval was not required for the study on human participants in accordance with the local legislation and institutional requirements. The patients/participants provided their written informed consent to participate in this study.

## AUTHOR CONTRIBUTIONS

HJ performed the experiments, compiled the data, and prepared the manuscript. MS assisted in experiments. HU helped in biological assays. MK helped in characterization of NPs. MZ helped in characterization of NPs. CH performed HPLC and reviewed the manuscript. BA supervised the research and critically reviewed the manuscript. All authors contributed to the article and approved the submitted version.

- Bylka, W., Frański, R., and Stobiecki, M. (2002). Differentiation between isomeric acacetin-6-C-(6 ?-O-malonyl) glucoside and acacetin-8-C-(6 ?-O-malonyl) glucoside by using low-energy CID mass spectra. *J. Mass Spectrom.* 37, 648–650. doi: 10.1002/jms.313
- Cai, X., Luo, Y., Zhang, W., Du, D., and Lin, Y. (2016). pH-Sensitive ZnO quantum dots-doxorubicin nanoparticles for lung cancer targeted drug delivery. *ACS Appl. Mater. Interf.* 8, 22442–22450. doi: 10.1021/acsami.6b04933
- Davar, F., Majedi, A., and Mirzaei, A. (2015). Green synthesis of ZnO nanoparticles and its application in the degradation of some dyes. *J. Am. Ceram. Soc.* 98, 1739–1746. doi: 10.1111/jace.13467
- Diallo, A., Ngom, B., Park, E., and Maaza, M. (2015). Green synthesis of ZnO nanoparticles by *Aspalathus linearis*: structural & optical properties. *J. Alloys Compounds* 646, 425–430. doi: 10.1016/j.jallcom.2015.05.242
- Duan, H., Wang, D., and Li, Y. (2015). Green chemistry for nanoparticle synthesis. *Chem. Soc. Rev.* 44, 5778–5792. doi: 10.1039/c4cs00363b
- Evans, B. C., Nelson, C. E., Shann, S. Y., Beavers, K. R., Kim, A. J., Li, H., et al. (2013). Ex vivo red blood cell hemolysis assay for the evaluation of pH-responsive endosomolytic agents for cytosolic delivery of biomacromolecular drugs. *JoVE* 2013:e50166.
- Fan, F., Feng, Y., Tang, P., and Li, D. (2015). Facile synthesis and photocatalytic performance of ZnO nanoparticles self-assembled spherical aggregates. *Mater. Lett.* 158, 290–294. doi: 10.1016/j.matlet.2015.05.109
- Fatima, H., Khan, K., Zia, M., Ur-Rehman, T., Mirza, B., and Haq, I.-U. (2015). Extraction optimization of medicinally important metabolites from *Datura innoxia* Mill.: an in vitro biological and phytochemical investigation. *BMC Complement. Altern. Med.* 15:376. doi: 10.1186/s12906-015-0891-1
- Hameed, A. S. H., Karthikeyan, C., Kumar, V. S., Kumaresan, S., and Sasikumar, S. (2015). Effect of Mg<sup>2+</sup>, Ca<sup>2+</sup>, Sr<sup>2+</sup> and Ba<sup>2+</sup> metal ions on the antifungal activity of ZnO nanoparticles tested against *Candida albicans*. *Mater. Sci. Eng. C* 52, 171–177. doi: 10.1016/j.msec.2015.03.030
- Hatamie, A., Khan, A., Golabi, M., Turner, A. P., Beni, V., Mak, W. C., et al. (2015). Zinc oxide nanostructure-modified textile and its application to biosensing, photocatalysis, and as antibacterial material. *Langmuir* 31, 10913–10921. doi: 10.1021/acs.langmuir.5b02341
- He, L., Liu, Y., Mustapha, A., and Lin, M. (2011). Antifungal activity of zinc oxide nanoparticles against *Botrytis cinerea* and *Penicillium expansum*. *Microbiol. Res.* 166, 207–215. doi: 10.1016/j.micres.2010.03.003
- Huang, J., Li, Q., Sun, D., Lu, Y., Su, Y., Yang, X., et al. (2007). Biosynthesis of silver and gold nanoparticles by novel sundried *Cinnamomum camphora* leaf. *Nanotechnology* 18:105104.

- Hussain, I., Bano, A., and Ullah, F. (2011). Traditional drug therapies from various medicinal plants of central karakoram national park, Gilgit-Baltistan Pakistan. *Pak. J. Bot.* 43, 79–84.
- Iravani, S. (2011). Green synthesis of metal nanoparticles using plants. *Green Chem.* 13, 2638–2650.
- Jamdnagi, P., Khatri, P., and Rana, J. (2018). Green synthesis of zinc oxide nanoparticles using flower extract of *Nyctanthes arbor-tristis* and their antifungal activity. *J. King Saud Univ. Sci.* 30, 168–175. doi: 10.1016/j.jksus.2016.10.002
- Jan, H., Khan, M. A., Usman, H., Shah, M., Ansir, R., Faisal, S., et al. (2020). The *Aquilegia pubiflora* (Himalayan columbine) mediated synthesis of nanoceria for diverse biomedical applications. *RSC Adv.* 10, 19219–19231. doi: 10.1039/d0ra01971b
- Janaki, A. C., Sailatha, E., and Gunasekaran, S. (2015). Synthesis, characteristics and antimicrobial activity of ZnO nanoparticles. *Spectrochimica acta Part A. Mol. Biomol. Spectrosc.* 144, 17–22. doi: 10.1016/j.saa.2015.02.041
- Jebali, A., and Kazemi, B. (2013). Nano-based antileishmanial agents: a toxicological study on nanoparticles for future treatment of *Cutaneous leishmaniasis*. *Toxicol. Vitro* 27, 1896–1904. doi: 10.1016/j.tiv.2013.06.002
- Khan, S. A., Noreen, F., Kanwal, S., Iqbal, A., and Hussain, G. (2018). Green synthesis of ZnO and Cu-doped ZnO nanoparticles from leaf extracts of *Abutilon indicum*, *Clerodendrum infortunatum*, *Clerodendrum inerme* and investigation of their biological and photocatalytic activities. *Mater. Sci. Eng. C* 82, 46–59. doi: 10.1016/j.msec.2017.08.071
- Król, A., Pomastowski, P., Rafińska, K., Railean-Plugaru, V., and Buszewski, B. (2017). Zinc oxide nanoparticles: synthesis, antiseptic activity and toxicity mechanism. *Adv. Colloid Interf. Sci.* 249, 37–52. doi: 10.1016/j.cis.2017.07.033
- Kumar, R., Al-Dossary, O., Kumar, G., and Umar, A. (2015). Zinc oxide nanostructures for NO<sub>2</sub> gas-sensor applications: a review. *Nano Micro Lett.* 7, 97–120. doi: 10.1007/s40820-014-0023-3
- Kumar, S. G., and Rao, K. K. (2015). Zinc oxide based photocatalysis: tailoring surface-bulk structure and related interfacial charge carrier dynamics for better environmental applications. *RSC Adv.* 5, 3306–3351. doi: 10.1039/c4ra13299h
- Lam, K. Y., Ling, A. P. K., Koh, R. Y., Wong, Y. P., and Say, Y. H. (2016). A review on medicinal properties of orientin. *Adv. Pharmacol. Sci.* 2016:4104595.
- Lipovsky, A., Nitzan, Y., Gedanken, A., and Lubart, R. (2011). Antifungal activity of ZnO nanoparticles—the role of ROS mediated cell injury. *Nanotechnology* 22:105101. doi: 10.1088/0957-4484/22/10/105101
- Mani, G. K., and Rayappan, J. B. B. (2015). Facile synthesis of ZnO nanostructures by spray pyrolysis technique and its application as highly selective H<sub>2</sub>S sensor. *Mater. Lett.* 158, 373–376. doi: 10.1016/j.matlet.2015.05.006
- Matinise, N., Fuku, X., Kaviyarasu, K., Mayedwa, N., and Maaza, M. (2017). ZnO nanoparticles via *Moringa oleifera* green synthesis: physical properties & mechanism of formation. *Appl. Surf. Sci.* 406, 339–347. doi: 10.1016/j.apsusc.2017.01.219
- Modena, M. M., Rühle, B., Burg, T. P., and Wuttke, S. (2019). Nanoparticle characterization: what to measure? *Adv. Mater.* 31:1901556. doi: 10.1002/adma.201901556
- Mushtaq, S., Aga, M. A., Qazi, P. H., and Ali, M. N. (2016). Isolation, characterization and HPLC quantification of compounds from *Aquilegia fragrans* Benth: their in vitro antibacterial activities against bovine mastitis pathogens. *J. Ethnopharmacol.* 178, 9–12. doi: 10.1016/j.jep.2015.11.039
- Naveed, M., Hejazi, V., Abbas, M., Kamboh, A. A., Khan, G. J., Shumzaid, M., et al. (2018). Chlorogenic acid (CGA): a pharmacological review and call for further research. *Biomed. Pharmacother.* 97, 67–74.
- Nazir, M., Tungmunthum, D., Bose, S., Drouet, S., Garros, L., Giglioli-Guivarc'h, N., et al. (2019). Differential production of phenylpropanoid metabolites in callus cultures of *Ocimum basilicum* L. with distinct in vitro antioxidant activities and in vivo protective effects against UV stress. *J. Agric. Food Chem.* 67, 1847–1859. doi: 10.1021/acs.jafc.8b05647
- Raghupathi, K. R., Koodali, R. T., and Manna, A. C. (2011). Size-dependent bacterial growth inhibition and mechanism of antibacterial activity of zinc oxide nanoparticles. *Langmuir* 27, 4020–4028. doi: 10.1021/la104825u
- Raoufi, D. (2013). Synthesis and microstructural properties of ZnO nanoparticles prepared by precipitation method. *Renew. Energy* 50, 932–937. doi: 10.1016/j.renene.2012.08.076
- Sangeetha, G., Rajeshwari, S., and Venkatesh, R. (2011). Green synthesis of zinc oxide nanoparticles by aloe barbadensis miller leaf extract: structure and optical properties. *Mater. Res. Bull.* 46, 2560–2566. doi: 10.1016/j.materresbull.2011.07.046
- Sankapal, B. R., Gajare, H. B., Karade, S. S., Salunkhe, R. R., and Dubal, D. P. (2016). Zinc oxide encapsulated carbon nanotube thin films for energy storage applications. *Electrochim. Acta* 192, 377–384. doi: 10.1016/j.electacta.2016.01.193
- Santos-Sánchez, N. F., Salas-Coronado, R., Hernández-Carlos, B., and Villanueva-Cañongo, C. (2019). “Shikimic acid pathway in biosynthesis of phenolic compounds,” in *Plant Physiological Aspects of Phenolic Compounds*, eds M. S. Hernández, R. G. Mateos and M. P. Tenango (London: IntechOpen).
- Shah, M., Nawaz, S., Jan, H., Uddin, N., Ali, A., Anjum, S., et al. (2020). Synthesis of bio-mediated silver nanoparticles from *Silybum marianum* and their biological and clinical activities. *Mater. Sci. Eng. C* 112:110889. doi: 10.1016/j.msec.2020.110889
- Sharma, D., Rajput, J., Kaith, B., Kaur, M., and Sharma, S. (2010). Synthesis of ZnO nanoparticles and study of their antibacterial and antifungal properties. *Thin Solid Films* 519, 1224–1229. doi: 10.1016/j.tsf.2010.08.073
- Sirelkhatim, A., Mahmud, S., Seeni, A., Kaus, N. H. M., Ann, L. C., Bakhori, S. K. M., et al. (2015). Review on zinc oxide nanoparticles: antibacterial activity and toxicity mechanism. *Nano Micro Lett.* 7, 219–242. doi: 10.1007/s40820-015-0040-x
- Sonker, R. K., Sabhajeet, S., Singh, S., and Yadav, B. (2015). Synthesis of ZnO nanoparticles and its application as NO<sub>2</sub> gas sensor. *Mater. Lett.* 152, 189–191. doi: 10.1016/j.matlet.2015.03.112
- Suntako, R. (2015). Effect of zinc oxide nanoparticles synthesized by a precipitation method on mechanical and morphological properties of the CR foam. *Bull. Mater. Sci.* 38, 1033–1038. doi: 10.1007/s12034-015-0921-0
- Suresh, D., Nethravathi, P., Rajanaika, H., Nagabhushana, H., and Sharma, S. (2015). Green synthesis of multifunctional zinc oxide (ZnO) nanoparticles using Cassia fistula plant extract and their photodegradative, antioxidant and antibacterial activities. *Mater. Sci. Semiconduct. Proc.* 31, 446–454. doi: 10.1016/j.mssp.2014.12.023
- Taş, A. C., Majewski, P. J., and Aldinger, F. (2000). Chemical preparation of pure and strontium-and/or magnesium-doped lanthanum gallate powders. *J. Am. Ceram. Soc.* 83, 2954–2960. doi: 10.1111/j.1151-2916.2000.tb01666.x
- Thatoi, P., Kerry, R. G., Gouda, S., Das, G., Pramanik, K., Thatoi, H., et al. (2016). Photo-mediated green synthesis of silver and zinc oxide nanoparticles using aqueous extracts of two mangrove plant species, *Heritiera fomes* and *Sonneratia apetala* and investigation of their biomedical applications. *J. Photochem. Photobiol. B Biol.* 163, 311–318. doi: 10.1016/j.jphotobiol.2016.07.029
- Thema, F., Manikandan, E., Dhilamini, M., and Maaza, M. (2015). Green synthesis of ZnO nanoparticles via *Agathosma betulina* natural extract. *Mater. Lett.* 161, 124–127. doi: 10.1016/j.matlet.2015.08.052
- Usman, H., Ullah, M. A., Jan, H., Siddiquah, A., Drouet, S., Anjum, S., et al. (2020). Interactive Effects of Wide-spectrum monochromatic lights on phytochemical production, antioxidant and biological activities of *Solanum xanthocarpum* callus cultures. *Molecules* 25:2201. doi: 10.3390/molecules25092201
- Uthirakumar, P., and Hong, C.-H. (2009). Effect of annealing temperature and pH on morphology and optical property of highly dispersible ZnO nanoparticles. *Mater. Charact.* 60, 1305–1310. doi: 10.1016/j.matchar.2009.06.002
- Vijayakumar, S., Vaseeharan, B., Malaikozhundan, B., and Shobiya, M. (2016). Laurus nobilis leaf extract mediated green synthesis of ZnO nanoparticles: characterization and biomedical applications. *Biomed. Pharmacother.* 84, 1213–1222. doi: 10.1016/j.biopha.2016.10.038
- Vijayalakshmi, U., Chellappa, M., Anjaneyulu, U., Manivasagam, G., and Sethu, S. (2016). Influence of coating parameter and sintering atmosphere on the corrosion resistance behavior of electrophoretically deposited composite coatings. *Mater. Manufact. Process.* 31, 95–106. doi: 10.1080/10426914.2015.1070424
- Vimala, K., Sundarraj, S., Paulpandi, M., Vengatesan, S., and Kannan, S. (2014). Green synthesized doxorubicin loaded zinc oxide nanoparticles regulates the Bax and Bcl-2 expression in breast and colon carcinoma. *Process Biochem.* 49, 160–172. doi: 10.1016/j.procbio.2013.10.007
- Wang, M.-H., Ma, X.-Y., and Zhou, F. (2015). Synthesis and characterization of monodispersed spherical ZnO nanocrystals in an aqueous solution. *Mater. Lett.* 142, 64–66. doi: 10.1016/j.matlet.2014.11.126

- Waters, B., Saxena, G., Wanggui, Y., Kau, D., Wrigley, S., Stokes, R., et al. (2002). Identifying protein kinase inhibitors using an assay based on inhibition of aerial hyphae formation in *Streptomyces*. *J. Antibiot.* 55, 407–416. doi: 10.7164/antibiotics.55.407
- Xie, Y., He, Y., Irwin, P. L., Jin, T., and Shi, X. (2011). Antibacterial activity and mechanism of action of zinc oxide nanoparticles against *Campylobacter jejuni*. *Appl. Environ. Microbiol.* 77, 2325–2331. doi: 10.1128/aem.02149-10
- Yao, G., Sebisubi, F. M., Voo, L. Y. C., Ho, C. C., Tan, G. T., and Chang, L. C. (2011). Citrinin derivatives from the soil filamentous fungus *Penicillium* sp. H9318. *J. Brazil. Chem. Soc.* 22, 1125–1129. doi: 10.1590/s0103-50532011000600018
- Yu, Y., Yi, Z.-B., and Liang, Y.-Z. (2007). Validate antibacterial mode and find main bioactive components of traditional Chinese medicine *Aquilegia oxysepala*. *Bioorgan. Med. Chem. Lett.* 17, 1855–1859. doi: 10.1016/j.bmcl.2007.01.032

**Conflict of Interest:** The authors declare that the research was conducted in the absence of any commercial or financial relationships that could be construed as a potential conflict of interest.

Copyright © 2020 Jan, Shah, Usman, Khan, Zia, Hano and Abbasi. This is an open-access article distributed under the terms of the Creative Commons Attribution License (CC BY). The use, distribution or reproduction in other forums is permitted, provided the original author(s) and the copyright owner(s) are credited and that the original publication in this journal is cited, in accordance with accepted academic practice. No use, distribution or reproduction is permitted which does not comply with these terms.